PCCP

PAPER

View Article Online
View Journal | View Issue

Cite this: *Phys. Chem. Chem. Phys.*, 2018, **20**, 10838

Kinetics of the reaction of $CO_3^{\bullet-}(H_2O)_n$, n = 0, 1, 2, with nitric acid, a key reaction in tropospheric negative ion chemistry†

Christian van der Linde, *[a] Wai Kit Tang, [b] Chi-Kit Siu *[b] and Martin K. Beyer *[a]

Received 17th November 2017,
Accepted 19th February 2018

DOI: 10.1039/c7cp07773d

rsc.li/pccp

A significant fraction of nitrate in the troposphere is formed in the reactions of HNO_3 with the carbonate radical anion $CO_3^{\bullet-}$ and the mono- and dihydrated species $CO_3^{\bullet-}(H_2O)_{1,2}$. A reaction mechanism was proposed in earlier flow reactor studies, which is investigated here in more detail by quantum chemical calculations and experimental reactivity studies of mass selected ions under ultra-high vacuum conditions. Bare $CO_3^{\bullet-}$ forms $NO_3^-(OH^\bullet)$ as well as NO_3^-, with a total rate coefficient of 1.0×10^{-10} cm^3 s^{-1}. $CO_3^{\bullet-}(H_2O)$ in addition affords stabilization of the $NO_3^-(HCO_3^\bullet)$ collision complex, and thermalized $CO_3^{\bullet-}(H_2O)$ reacts with a total rate coefficient of 6.3×10^{-10} cm^3 s^{-1}. A second solvent molecule quenches the reaction, and only black-body radiation induced dissociation is observed for $CO_3^{\bullet-}(H_2O)_2$, with an upper limit of 6.0×10^{-11} cm^3 s^{-1} for any potential bimolecular reaction channel. The rate coefficients obtained under ultra-high vacuum conditions are smaller than in the earlier flow reactor studies, due to the absence of stabilizing collisions, which also has a strong effect on the product branching ratio. Quantum chemical calculations corroborate the mechanism proposed by Möhler and Arnold. The reaction proceeds through a proton-transferred $NO_3^-(HCO_3^\bullet)$ collision complex, which can rearrange to $NO_3^-(OH^\bullet)(CO_2)$. The weakly bound CO_2 easily evaporates, followed by evaporation of the more strongly attached $OH^\bullet$, if sufficient energy is available.

Introduction

The $CO_3^{\bullet-}$ radical anion is an important intermediate in the tropospheric chemistry of anions.[1,2] Quantitative modeling by Kawamoto *et al.*[3] places the fractional abundance of $CO_3^{\bullet-}$ core ions in the troposphere in the range of 0.9–2.3%, quite comparable to HSO_4^- core ions close to the ground, while the overwhelming majority of negative ions have an NO_3^- core. However, a significant fraction of $NO_3^-(H_2O)$ is formed in the reaction of $CO_3^{\bullet-}(H_2O)$ with HNO_3.[3] In recent years, ions in the troposphere have received increased attention in the form of charged aerosol particles.[4] In a series of laboratory experiments, the CLOUD collaboration at CERN has recently shown that ions play an important role for aerosol nucleation and cloud formation in the troposphere.[5–8]

The formation of $CO_3^{\bullet-}$ in atmospheric conditions was described by Fehsenfeld, Ferguson and co-workers in the 1970s.[9] In the first step electrons react with O_2 and an additional collision partner M to form O_2^-, reaction (1). Ozonide $O_3^{\bullet-}$ is formed by charge transfer to an ozone molecule, reaction (2). The ozonide anion finally transfers O^- to a carbon dioxide molecule, forming $CO_3^{\bullet-}$ and O_2, reaction (3).

$$e^- + O_2 + M \rightarrow O_2^{\bullet-} + M,\ M = O_2, N_2, Ar, H_2O, \ldots \quad (1)$$

$$O_2^{\bullet-} + O_3 \rightarrow O_2 + O_3^{\bullet-} \quad (2)$$

$$O_3^{\bullet-} + CO_2 \rightarrow CO_3^{\bullet-} + O_2 \quad (3)$$

The properties of $CO_3^{\bullet-}$ itself were intensively studied by spectroscopy. Matrix isolation techniques were applied by Jacox *et al.*,[10] and a number of other groups used photodissociation techniques to characterize $CO_3^{\bullet-}$.[11–14] The O_2C–O^- bond dissociation energy was determined by Johnson, Viggiano and co-workers *via* photodissociation and high level quantum chemical calculations to be 269 ± 5 kJ mol^{-1}.[15–17]

Despite its key role in tropospheric anion chemistry,[18] only a small number of gas phase reactions were studied.[19–23] These are mostly reactions with nitrogen oxides, leading to formation

[a] *Institut für Ionenphysik und Angewandte Physik, Universität Innsbruck, Technikerstraße 25, 6020 Innsbruck, Austria. E-mail: christian.van-der-linde@uibk.ac.at, martin.beyer@uibk.ac.at*
[b] *Department of Chemistry, City University of Hong Kong, 83 Tat Chee Avenue, Kowloon Tong, Hong Kong SAR, P. R. China. E-mail: chiksiu@cityu.edu.hk*

† Electronic supplementary information (ESI) available. See DOI: 10.1039/c7cp07773d

of nitrate NO_3^-.[3,24–27] Reactions of $CO_3^-(H_2O)_{0,1,2}$ with formic, acetic, propionic, butyric, glyoxylic, pyruvic and pinonic acid were investigated in a flow tube experiment by Arnold *et al.*[28,29] They reported as initial step mostly proton transfer giving the deprotonated acids as products. For propionic acid and larger, they also observed clustering with $CO_3^{\bullet-}$ and formation of radical species, *e.g.* $CH_3CH(^\bullet)COO^-$ from propionic acid.[28,29] However, we recently showed that the reaction with formic acid proceeds mostly *via* oxidation of formic acid to carbon dioxide and water.[30] The deprotonation product $HCOO^-$ was re-assigned to the reaction of formic acid with $HCOO^-(OH^\bullet)$, an intermediate in the oxidation reaction that is formed in small concentrations.

A similar pattern emerged for the reaction of $CO_3^{\bullet-}$ with HCl. A flow tube study by Dotan *et al.*[24] established an upper limit for the rate of 3×10^{-11} cm^3 s^{-1}, without observing any products. Recent studies in our laboratory reveal that this reaction proceeds *via* formation of a short lived, very reactive $Cl^-(OH^\bullet)$ intermediate that reacts fast with a second HCl molecule, producing HCl_2^- and $Cl_2^{\bullet-}$ as final products.[31] The rate of the first step is 4.2×10^{-12} cm^3 s^{-1}, consistent with the upper limit given by Dotan *et al.*[24] Interestingly, hydration dramatically accelerates the rate to 2.7×10^{-10} cm^3 s^{-1} for $CO_3^{\bullet-}(H_2O)$, resulting in the reactive $Cl^-(HCO_3^\bullet)$ radical species.[31]

Nitric acid[21–23,32] and methane sulfonic acid[20] show efficient reactions with $CO_3^{\bullet-}$. The gas phase ion chemistry of HNO_3 was extensively investigated by Fehsenfeld and coworkers.[21] They reported a reaction rate coefficient of 8×10^{-10} cm^3 s^{-1} for reaction (4), measured by the flowing afterglow technique.

$$CO_3^{\bullet-} + HNO_3 \rightarrow NO_3^- + [CO_2,OH^\bullet] \quad (4)$$

Möhler and Arnold investigated the reaction of HNO_3 with $CO_3^{\bullet-}$ and $CO_3^{\bullet-}(H_2O)$ in a flow-reactor triple quadrupole mass spectrometer in the presence of 1.7 mbar N_2 and 0.3 mbar O_2 as buffer gas.[22] For bare $CO_3^{\bullet-}$ they observed NO_3^-, $[NO_3,OH^\bullet]^-$ and $[CO_3^\bullet,HNO_3]^-$ as primary products, followed by clustering reactions with HNO_3.[22] No $[NO_3,OH^\bullet]^-$ was observed when 0.03 mbar H_2O was added to the buffer gas to study the hydrated species, while $[CO_3^\bullet,HNO_3]^-$ was the dominant product.[22] A mechanism *via* an excited collision complex $[(CO_3^\bullet HNO_3)^-]^*$ was proposed. The complex is de-exited by collisions, or decays into NO_3^- or $[NO_3,OH^\bullet]^-$.[22] Catoire and co-workers used the $CO_3^{\bullet-}$ + HNO_3 reaction for testing their flowing afterglow setup and observed the same primary products as Möhler and Arnold.[22,32] Since no mass selection was available for the reactant ions, the exact sequence of reactions generating the observed products, in particular the role of the $[NO_3,OH^\bullet]^-$ and the influence of an additional water molecule on the reactivity, remained unclear.

Because of its central role in tropospheric negative ion chemistry,[1,3] we investigated the reaction of $CO_3^{\bullet-}(H_2O)_n$, n = 0, 1, 2, with HNO_3 by FT-ICR mass spectrometry and quantum chemical calculations. Each cluster size was studied separately with mass-selected ions. The extremely low pressure in the FT-ICR instrument leads to product distributions different from the flow reactor studies, due to the absence of stabilizing collisions. A key problem in gas-phase reactivity studies with HNO_3 is the inherent instability of this substance. HNO_3 decomposes in concentrated aqueous solutions. In earlier studies on the reactivity of ionic water clusters,[33–35] we worked with aqueous concentrated solutions of HNO_3, which yields a mixture of HNO_3 and H_2O in the reaction region, with traces of the decomposition product HONO. The observed reaction products confirmed that the abundance of HONO was less than 3% of the HNO_3 partial pressure. To identify reactions where HONO might play a role, we use quantum chemical calculations to identify thermochemically allowed reaction pathways. In addition, structural as well as thermochemical information is obtained for stationary points on the reaction potential energy surface. Together, a consistent picture of the reaction mechanism evolves.

Computational and experimental details

The ion–molecule reaction profiles were simulated with density functional theory at the M06-2X/6-311++G(d,p) level of theory employing the Gaussian09 program suite.[36] The energies of all optimized geometries were corrected with zero-point energy obtained from harmonic vibration analyses. Local minima and transition structures on the potential energy surface were confirmed with absence of and presence of one imaginary frequency, respectively. The local minima associated with each transition structure were verified by the intrinsic reaction coordinate (IRC) method. Spin density distributions were evaluated at the same level of theory and shown as isosurfaces at a value of 0.01 a.u. Table S1 in ESI,† compares the used methods/basis sets with experimental values. The coordinates are given in Table S4 (ESI†).

The experiments were performed on a modified Bruker/Spectrospin CMS47X FT-ICR mass spectrometer as described in detail elsewhere.[37–39] The spectrometer is equipped with a Bruker Infinity Cell, an APEX III data station, a 4.7 Tesla magnet and an external laser vaporization ion source. $CO_3^{\bullet-}$ was produced in the laser vaporization ion source[39–42] *via* expansion of a helium/water/oxygen/carbon dioxide mixture using a zinc target for the production of electrons. As vaporization laser a frequency doubled Nd:YAG laser at a pulse energy of $\sim$5 mJ at 10 Hz was used. All produced anionic species were transferred into the ICR cell, where they can be stored for several seconds or minutes. The ion of interest, $CO_3^{\bullet-}$ or $CO_3^{\bullet-}(H_2O)_{1,2}$, was then isolated *via* resonant excitation of unwanted ions prior to measuring the kinetics. A constant background pressure of HNO_3 and H_2O (concentrated aqueous solution, 70% HNO_3, Sigma-Aldrich) was introduced into the ultrahigh vacuum region *via* a leak valve. Due to the inherent instability of HNO_3, also traces of HONO were present, which are formed from the $NO_2^\bullet$ decomposition product on thin films of H_2O and HNO_3, as present in the vacuum system.[43] Mass spectra were taken after different reaction delays relative to the end of the fill and isolation cycle. The intensities were extracted from the mass spectra. A rate coefficient matrix defines the allowed reaction channels and the data was fitted using a genetic algorithm that optimizes the rates from the

matrix based on a pseudo-first order rate law. Relative rate coefficients were extracted from this fit. The stability of the fit was tested by systematically changing each parameter in 5 to 10 steps of ±5% from its optimized value, and re-optimizing all other parameters. The resulting error was plotted against the modified parameter. These plots are available as supporting information in Fig. S8 and S9 (ESI†). All rate coefficients reported in the results section showed stable, well-converged minima.

These pressure-dependent pseudo-first order rate coefficients are converted to pressure-independent bimolecular rate coefficients. An aqueous 70% HNO_3 solution is close to the azeotropic point and the chemical composition in the gas phase is therefore close to 70% HNO_3 and 30% water. As the cold cathode pressure gauge shows different sensitivity toward HNO_3 and H_2O, the measured pressure was corrected taking the different sensitivity into account. The HNO_3 partial pressure was taken as 70% of the corrected total pressure. More details on the kinetic analysis and pressure correction are available in ESI.† The accuracy of the absolute rates is estimated to be ±40% due to uncertainties in the pressure determination. The noise level is derived from the baseline of each mass spectrum.

Results and discussion

Calculated reaction potential energy surface

The potential energy surface (PES) corresponding to the reaction mechanisms suggested by Möhler and Arnold[22] is shown in Fig. 1. The calculations show that a barrierless proton transfer takes place upon formation of the collision complex **1**, which can be written as $NO_3^-(HCO_3^\bullet)$. Rearrangement of the $HCO_3^\bullet$ unit to CO_2 + $OH^\bullet$ within the complex faces a significant barrier of 81 kJ mol^{-1} *via* **TS1** located at −63 kJ mol^{-1} relative to the separated reactants. Evaporation of CO_2 from complex **2**, which can be written as $NO_3^-(OH^\bullet)(CO_2)$, requires only 33 kJ mol^{-1}, leading to the observed $NO_3^-(OH^\bullet)$ product. Further evaporation of the $OH^\bullet$ radical requires 68 kJ mol^{-1}, making the overall reaction with −3 kJ mol^{-1} below the entrance channel almost thermoneutral.

The water binding energies in $CO_3^{\bullet-}(H_2O)_{1,2}$ are 62 kJ mol^{-1} and 52 kJ mol^{-1} for the first and second molecule, respectively. Upon collision with HNO_3, the water molecules from $CO_3^-(H_2O)$ and $CO_3^-(H_2O)_2$ evaporate due to the energy released upon formation of the collision complex, since the transition states for rearrangement prior to water evaporation lie significantly higher in energy, see Fig. S1 (ESI†). For $CO_3^{\bullet-}(H_2O)$, the pathway to $NO_3^-(OH^\bullet)$ + CO_2 formation is still accessible, while bare NO_3^- formation is clearly out of reach, lying 59 kJ mol^{-1} above the $CO_3^{\bullet-}(H_2O)$ + HNO_3 entrance channel. The second water molecule reduces the available energy further, only the formation of the $NO_3^-(HCO_3^\bullet)$ complex **1** is thermochemically allowed, with a moderate exothermicity of −30 kJ mol^{-1}.

Experimental results and discussion

CO_3^-. The kinetics of the reaction of $CO_3^{\bullet-}$ with HNO_3 is displayed in Fig. 2. A mass spectrum is available in Fig. S5 (ESI†). The decay of the $CO_3^{\bullet-}$ ion intensity follows a pseudo-first order kinetics behavior. Primary reactions for pure $CO_3^{\bullet-}$ with the reaction mixture lead to formation of HCO_3^-, NO_3^-, and $NO_3^-(OH^\bullet)$. Rate coefficients for all reactions are given in Table 1. Compared to the flow reactor studies, the reaction is an order of magnitude slower, with an overall rate for all reaction channels of 1.0 × 10^{-10} cm^3 s^{-1}. Fehsenfeld *et al.*[21] reported a value of 8 × 10^{-10} cm^3 s^{-1} in their flowing afterglow, while Möhler and Arnold[22] agreed with their value of 1.3 × 10^{-9} cm^3 s^{-1} within error limits with Guimbaud *et al.*,[32] who reported 1.2 ± 0.3 × 10^{-9} cm^3 s^{-1}. Obviously, stabilizing collisions with the buffer gas in the flow reactor studies increase the efficiency of the reaction. The nitrate–hydroxyl radical complex arises from the reaction with gaseous HNO_3 according to reaction (5). Formation of HCO_3^- requires a hydrogen atom transfer (HAT), which is significantly endothermic for HNO_3, reaction (6). We therefore assign this small product to traces of HONO, reaction (7),

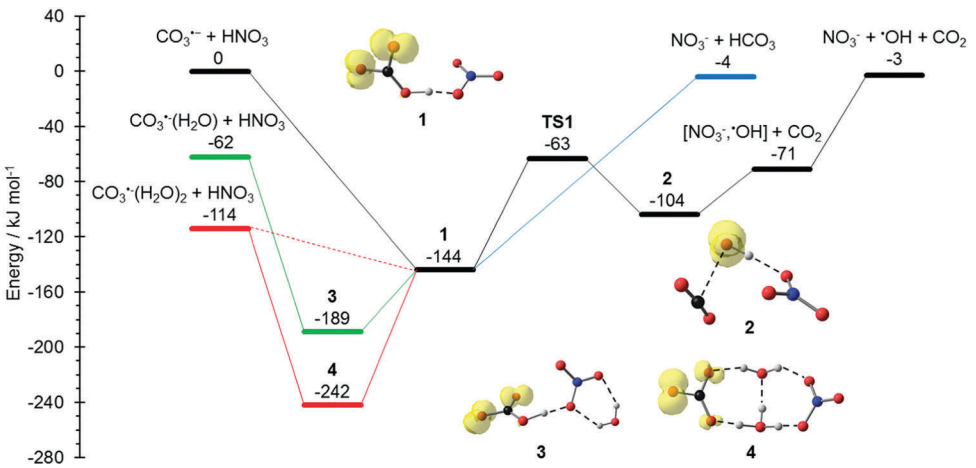

Fig. 1 Reaction potential energy surface (PES) calculated on the M06-2X/6-311++G(d,p) level of theory, with zero-point corrected energies given in kJ mol^{-1}. More detailed results on the influence of solvation and additional reaction channels are given in the ESI,† Fig. S1–S4.

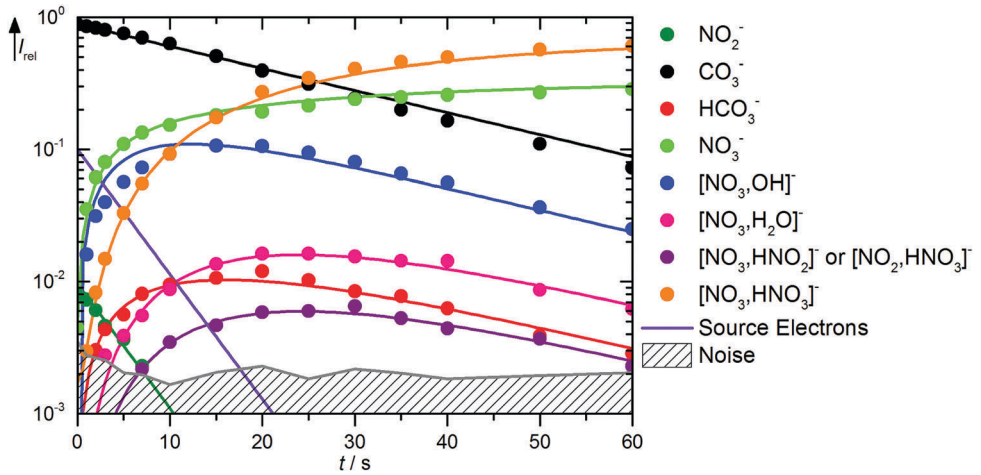

Fig. 2 Kinetics of the reaction of $CO_3^{\bullet-}$ with HNO_3 and H_2O, with traces of HONO, at a HNO_3 partial pressure of 1.4×10^{-8} mbar. The lines represent the fit with the rate coefficients from Table S1 (ESI†). Selected mass spectra are shown in Fig. S5 (ESI†).

Table 1 Bimolecular rate coefficients k_{abs} for the reactions discussed in the text

Reaction		Rate coefficient k_{abs}/cm^3 s^{-1}
(5)	$CO_3^{\bullet-} + HNO_3 \rightarrow NO_3^-(OH^\bullet) + CO_2$	8.9×10^{-11}
(8/9)	$CO_3^{\bullet-} + HNO_3 \rightarrow NO_3^- + [CO_2,OH^\bullet]$	2.1×10^{-11}
(10)	$HCO_3^- + HNO_3 \rightarrow NO_3^- + CO_2 + H_2O$	2.8×10^{-10}
(11)	$NO_3^-(OH^\bullet) + H_2O \rightarrow NO_3^-(H_2O) + OH^\bullet$	1.2×10^{-10} [a]
(12)	$NO_3^-(OH^\bullet) + HNO_3 \rightarrow NO_3^-(H_2O) + NO_3$	5.3×10^{-11} [a]
(14)	$NO_3^-(OH^\bullet) + HNO_3 \rightarrow NO_3^-(HNO_3) + OH^\bullet$	3.6×10^{-10}
(16)	$NO_2^- + HNO_3 \rightarrow NO_3^- + HONO$	7.2×10^{-9}
(18)	$CO_3^{\bullet-}(H_2O) + HNO_3 \rightarrow NO_3^-(OH^\bullet) + CO_2 + H_2O$	1.4×10^{-10} [b]
(19)	$CO_3^{\bullet-}(H_2O) + HNO_3 \rightarrow NO_3^-(HCO_3^\bullet) + H_2O$	9.4×10^{-11} [c] 1.4×10^{-10} [b]
(20)	$CO_3^{\bullet-}(H_2O) + HNO_3 \rightarrow NO_3^- + CO_2 + OH^\bullet + H_2O$	3.8×10^{-10} [b]

[a] Assuming either reaction (11) or (12). [b] Thermalized fraction of $CO_3^{\bullet-}(H_2O)$. [c] Cold fraction of $CO_3^{\bullet-}(H_2O)$; the accuracy of the absolute rates is estimated to be ±40% due to uncertainties in the pressure determination.

which is exothermic. The calculations show a barrierless HAT from HONO to CO_3^-. If we assume collision efficiency for reaction (7), a partial pressure below 1×10^{-10} mbar of the HONO background is sufficient to explain the observed abundance of HCO_3^-.

$$CO_3^{\bullet-} + HNO_3 \rightarrow NO_3^-(OH^\bullet) + CO_2 \quad \Delta H_0 = -71 \text{ kJ mol}^{-1} \quad (5)$$

$$CO_3^{\bullet-} + HNO_3 \rightarrow HCO_3^- + NO_3^\bullet \quad \Delta H_0 = +48 \text{ kJ mol}^{-1} \quad (6)$$

$$CO_3^{\bullet-} + HONO \rightarrow HCO_3^- + NO_2^\bullet \quad \Delta H_0 = -68 \text{ kJ mol}^{-1} \quad (7)$$

Formation of NO_3^- *via* reactions (8) or (9) with HNO_3 as neutral reactant is only slightly exothermic. Given that both reactants have low-lying vibrational modes, some extra thermal energy is available, which makes the reactions entirely plausible.

$$CO_3^{\bullet-} + HNO_3 \rightarrow NO_3^- + CO_2 + OH^\bullet \quad \Delta H_0 = -3 \text{ kJ mol}^{-1} \quad (8)$$

$$CO_3^{\bullet-} + HNO_3 \rightarrow NO_3^- + HCO_3^\bullet \quad \Delta H_0 = -4 \text{ kJ mol}^{-1} \quad (9)$$

According to our kinetics fit, several secondary reactions are observed. HCO_3^- reacts to NO_3^-, most likely *via* a straightforward proton transfer from HNO_3, reaction (10).

$$HCO_3^- + HNO_3 \rightarrow NO_3^- + CO_2 + H_2O \quad \Delta H_0 = -88 \text{ kJ mol}^{-1} \quad (10)$$

$NO_3^-(OH^\bullet)$ either undergoes ligand exchange with H_2O or HAT from HNO_3 to form $NO_3^-(H_2O)$, reactions (11) or (12), respectively. Ligand exchange is also possible with HONO as well as HNO_3, reactions (13) and (14), respectively. Since reactions (12) and (14) compete with each other, with reaction (14) being both more exothermic and mechanistically favorable, ligand exchange with water is the most plausible origin of the $NO_3^-(H_2O)$ product, reaction (11). Reaction (13) validates the presence of HONO in the reaction mixture.

$$NO_3^-(OH^\bullet) + H_2O \rightarrow NO_3^-(H_2O) + OH^\bullet \quad \Delta H_0 = +3 \text{ kJ mol}^{-1} \quad (11)$$

$$NO_3^-(OH^\bullet) + HNO_3 \rightarrow NO_3^-(H_2O) + NO_3 \quad \Delta H_0 = -34 \text{ kJ mol}^{-1} \quad (12)$$

$$NO_3^-(OH^\bullet) + HONO \rightarrow NO_3^-(HONO) + OH^\bullet \quad \Delta H_0 = -40 \text{ kJ mol}^{-1} \quad (13)$$

$$NO_3^-(OH^\bullet) + HNO_3 \rightarrow NO_3^-(HNO_3) + OH^\bullet \quad \Delta H_0 = -75 \text{ kJ mol}^{-1} \quad (14)$$

We also observe traces of NO_2^-, which are assigned to dissociative electron attachment. When working with negative ions, some free electrons are usually trapped in the ICR cell,[44] which react with HNO_3 according to reaction (15).[21] In turn, NO_2^- is converted with near collision rate to NO_3^- *via* proton transfer from HNO_3, reaction (16).

$$e^- + HNO_3 \rightarrow NO_2^- + OH^\bullet \quad (15)$$

$$NO_2^- + HNO_3 \rightarrow NO_3^- + HONO \quad (16)$$

$CO_3^{\bullet-}(H_2O)$. Fig. 3 shows the kinetics of the monohydrated species, mass spectra are displayed in Fig. S6 (ESI†). The scenario is quite complex, with a pronounced deviation of the $CO_3^{\bullet-}(H_2O)$ intensity from pseudo-first order behavior, for which a linear graph in the semi-logarithmic plot is expected. To describe the observed curvature, the population of this species is divided into two fractions, which correspond to the initially cold ions directly from the supersonic expansion, and the thermalized ions after heating by ambient black-body radiation and collision with the reaction gas. These effects are included in the kinetic model by allowing the cold fraction to be converted to the thermalized fraction, with a unimolecular rate treated as a fit parameter. Heating ultimately leads to formation of $CO_3^{\bullet-}$ *via* black-body infrared radiative dissociation (BIRD),[45–58] reaction (17), with a lifetime of 3 s for the thermalized fraction. This reaction is not allowed for the cold fraction in the kinetic model, see Table S2 (ESI†). Since the major part of the $CO_3^{\bullet-}(H_2O)$ population is already thermalized at nominally $t = 0$ s, and the thermalized fraction reacts overall much faster than the cold fraction, the intensity drop of $CO_3^{\bullet-}(H_2O)$ is faster in the beginning, and levels off at later times because the conversion from the cold to the hot fraction becomes rate limiting, which explains the observed curvature.

The formation of $NO_3^-(OH^\bullet)$ is observed with an appreciable rate, and can be assigned to collisions with HNO_3, reaction (18). Also the transition state for CO_2 formation is below the entrance channel, see Fig. 1, thus reaction (18) is fully consistent with the calculations. The same is true for the ligand exchange product $NO_3^-(HCO_3^\bullet)$ formed *via* reaction (19). NO_3^- is exclusively formed from the thermalized fraction of $CO_3^{\bullet-}(H_2O)$ as a primary product in the kinetics. With HNO_3 as the reaction partner, reaction (20) is with $\Delta H_0 = +59$ kJ mol^{-1} significantly endothermic. However, the thermalized fraction of $CO_3^{\bullet-}(H_2O)$ already contains almost enough energy for dissociation. Together with the internal energy of the HNO_3 collision partner, the energy required for reaction (20) is available in the system. Reactions (18)–(20) yield a total rate coefficient of 6.3×10^{-10} cm^3 s^{-1} for the reaction of thermalized $CO_3^{\bullet-}(H_2O)$ with HNO_3, 37% of the flow reactor value of 1.7×10^{-9} cm^3 s^{-1} reported by Möhler and Arnold.[22] All secondary reactions as well as NO_2^- formation *via* dissociative electron attachment proceed as discussed above.

$$CO_3^{\bullet-}(H_2O) \rightarrow CO_3^{\bullet-} + H_2O \quad \Delta H_0 = +62 \text{ kJ mol}^{-1} \quad (17)$$

$$CO_3^{\bullet-}(H_2O) + HNO_3 \rightarrow NO_3^-(OH^\bullet) + CO_2 + H_2O \quad \Delta H_0 = -9 \text{ kJ mol}^{-1} \quad (18)$$

$$CO_3^{\bullet-}(H_2O) + HNO_3 \rightarrow NO_3^-(HCO_3^\bullet) + H_2O \quad \Delta H_0 = -83 \text{ kJ mol}^{-1} \quad (19)$$

$$CO_3^{\bullet-}(H_2O) + HNO_3 \rightarrow NO_3^- + CO_2 + OH^\bullet + H_2O \quad \Delta H_0 = +59 \text{ kJ mol}^{-1} \quad (20)$$

$CO_3^{\bullet-}(H_2O)_2$. Solvation of $CO_3^{\bullet-}$ with two water molecules leads to a significantly reduced reactivity with HNO_3. The kinetics is shown in Fig. 4, mass spectra are available in Fig. S7 (ESI†). The major reaction channel is, as might be expected, loss of a water molecule due to BIRD, reaction (21). There is again formation of NO_2^- *via* reaction (15), but otherwise no primary products are observed from $CO_3^{\bullet-}(H_2O)_2$. The noise level of the kinetics, however, places a high upper limit of 6.0×10^{-11} cm^3 s^{-1} on the rate coefficient for the direct reaction of $CO_3^{\bullet-}(H_2O)_2$ with HNO_3. According to the thermochemical arguments discussed above, the most likely product of such a

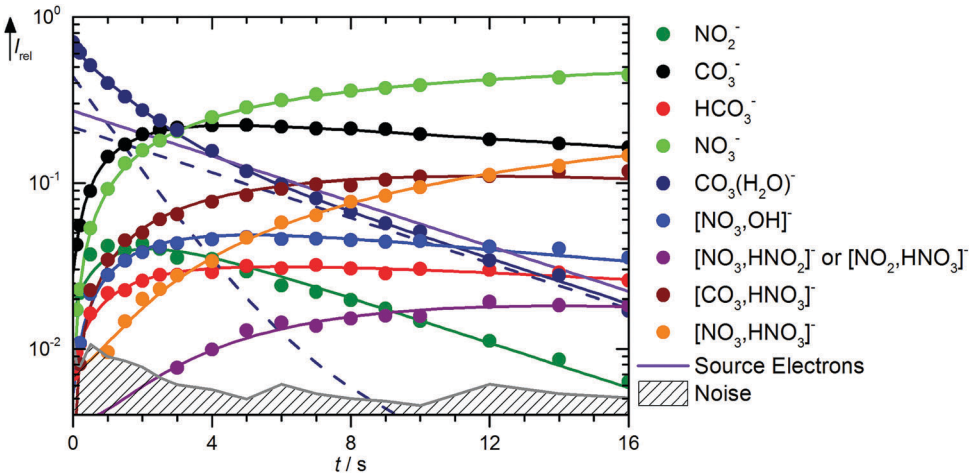

Fig. 3 Kinetics of the reaction of $CO_3^{\bullet-}(H_2O)$ with HNO_3 and H_2O, with traces of HONO, at a HNO_3 partial pressure of 2.1×10^{-8} mbar. The lines represent the fit with the rate coefficients from Table S2 (ESI†). Selected mass spectra are shown in Fig. S6 (ESI†).

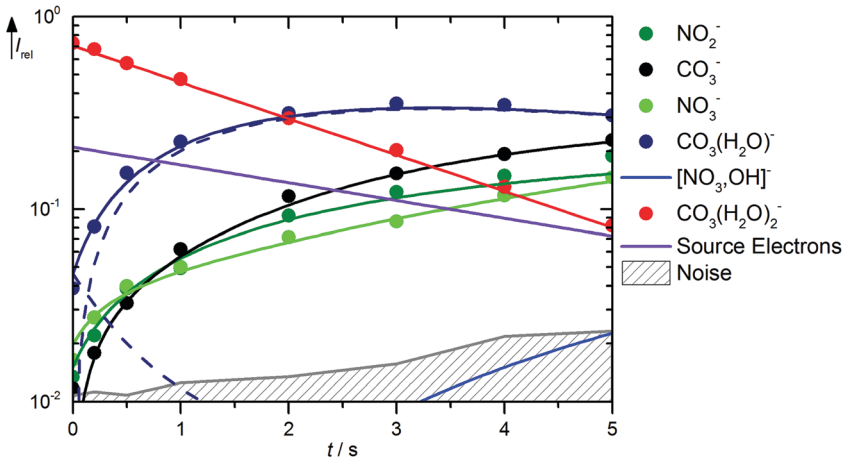

Fig. 4 Kinetics of the reaction of $CO_3^{\bullet-}(H_2O)_2$ with HNO_3 and H_2O, with traces of HONO, at a HNO_3 partial pressure of 8.1×10^{-9} mbar. The lines represent the fit with the rate coefficients from Table S3 (ESI†). Selected mass spectra are shown in Fig. S7 (ESI†).

reaction would be $NO_3^-(HCO_3^{\bullet})$, followed by $NO_3^-(OH^{\bullet})$, while direct NO_3^- formation this time is clearly out of reach.

$$CO_3^{\bullet-}(H_2O)_2 \rightarrow CO_3^{\bullet-}(H_2O) + H_2O \quad \Delta H_0 = +52 \text{ kJ mol}^{-1} \quad (21)$$

Conclusions

The mechanism of the reaction of HNO_3 with $CO_3^{\bullet-}(H_2O)_n$, $n = 0$, 1, 2, is very similar to the previously studied HCl reaction.[31] With bare $CO_3^{\bullet-}$, the reaction is relatively slow, and the proton-transfer intermediate $NO_3^-(OH^{\bullet})$ is the unambiguously identified primary product, corresponding to $Cl^-(OH^{\bullet})$ in the HCl reaction. Also NO_3^- is directly formed, but with even lower rate. Formation of $NO_3^-(OH^{\bullet})$ is accelerated for $CO_3^{\bullet-}(H_2O)$, but again slowed down by a second water molecule in the hydration shell. The rate is clearly dependent on the number of water molecules solvating $CO_3^{\bullet-}$, and overall significantly lower than in the flow reactor studies previously reported in the literature, indicating a strong pressure dependence.

Conflicts of interest

There are no conflicts to declare.

Acknowledgements

M. K. B. acknowledges startup funds from the University of Innsbruck. C. K. S. thanks Research Grants Council, Hong Kong SAR (Project no. 11300917) and City University of Hong Kong (CityU) (Project no. 7004401) for their financial support. W. K. T. acknowledges Chow Yei Ching School of Graduate Studies, CityU for his postgraduate studentships, outstanding academic performance awards, research tuition scholarships and overseas research activities award.

References

1 G. Beig and G. P. Brasseur, *J. Geophys. Res.: Atmos.*, 2000, **105**, 22671–22684.
2 M. L. Huertas, J. Fontan and J. Gonzalez, *Atmos. Environ.*, 1978, **12**, 2351–2362.
3 H. Kawamoto and T. Ogawa, *Planet. Space Sci.*, 1986, **34**, 1229–1239.
4 A. Hirsikko, T. Nieminen, S. Gagné, K. Lehtipalo, H. E. Manninen, M. Ehn, U. Hõrrak, V.-M. Kerminen, L. Laakso, P. H. McMurry, A. Mirme, S. Mirme, T. Petäjä, H. Tammet, V. Vakkari, M. Vana and M. Kulmala, *Atmos. Chem. Phys.*, 2011, **11**, 767–798.
5 J. Kirkby, J. Duplissy, K. Sengupta, C. Frege, H. Gordon, C. Williamson, M. Heinritzi, M. Simon, C. Yan, J. Almeida, J. Tröstl, T. Nieminen, I. K. Ortega, R. Wagner, A. Adamov, A. Amorim, A.-K. Bernhammer, F. Bianchi, M. Breitenlechner, S. Brilke, X. Chen, J. Craven, A. Dias, S. Ehrhart, R. C. Flagan, A. Franchin, C. Fuchs, R. Guida, J. Hakala, C. R. Hoyle, T. Jokinen, H. Junninen, J. Kangasluoma, J. Kim, M. Krapf, A. Kürten, A. Laaksonen, K. Lehtipalo, V. Makhmutov, S. Mathot, U. Molteni, A. Onnela, O. Peräkylä, F. Piel, T. Petäjä, A. P. Praplan, K. Pringle, A. Rap, N. A. D. Richards, I. Riipinen, M. P. Rissanen, L. Rondo, N. Sarnela, S. Schobesberger, C. E. Scott, J. H. Seinfeld, M. Sipilä, G. Steiner, Y. Stozhkov, F. Stratmann, A. Tomé, A. Virtanen, A. L. Vogel, A. C. Wagner, P. E. Wagner, E. Weingartner, D. Wimmer, P. M. Winkler, P. Ye, X. Zhang, A. Hansel, J. Dommen, N. M. Donahue, D. R. Worsnop, U. Baltensperger, M. Kulmala, K. S. Carslaw and J. Curtius, *Nature*, 2016, **533**, 521–526.
6 K. Lehtipalo, L. Rondo, J. Kontkanen, S. Schobesberger, T. Jokinen, N. Sarnela, A. Kürten, S. Ehrhart, A. Franchin, T. Nieminen, F. Riccobono, M. Sipilä, T. Yli-Juuti, J. Duplissy, A. Adamov, L. Ahlm, J. Almeida, A. Amorim, F. Bianchi, M. Breitenlechner, J. Dommen, A. J. Downard, E. M. Dunne, R. C. Flagan, R. Guida, J. Hakala, A. Hansel, W. Jud, J. Kangasluoma, V.-M. Kerminen, H. Keskinen,

J. Kim, J. Kirkby, A. Kupc, O. Kupiainen-Määttä, A. Laaksonen, M. J. Lawler, M. Leiminger, S. Mathot, T. Olenius, I. K. Ortega, A. Onnela, T. Petäjä, A. Praplan, M. P. Rissanen, T. Ruuskanen, F. D. Santos, S. Schallhart, R. Schnitzhofer, M. Simon, J. N. Smith, J. Tröstl, G. Tsagkogeorgas, A. Tomé, P. Vaattovaara, H. Vehkamäki, A. E. Vrtala, P. E. Wagner, C. Williamson, D. Wimmer, P. M. Winkler, A. Virtanen, N. M. Donahue, K. S. Carslaw, U. Baltensperger, I. Riipinen, J. Curtius, D. R. Worsnop and M. Kulmala, *Nat. Commun.*, 2016, **7**, 11594.

7 J. Tröstl, W. K. Chuang, H. Gordon, M. Heinritzi, C. Yan, U. Molteni, L. Ahlm, C. Frege, F. Bianchi, R. Wagner, M. Simon, K. Lehtipalo, C. Williamson, J. S. Craven, J. Duplissy, A. Adamov, J. Almeida, A.-K. Bernhammer, M. Breitenlechner, S. Brilke, A. Dias, S. Ehrhart, R. C. Flagan, A. Franchin, C. Fuchs, R. Guida, M. Gysel, A. Hansel, C. R. Hoyle, T. Jokinen, H. Junninen, J. Kangasluoma, H. Keskinen, J. Kim, M. Krapf, A. Kürten, A. Laaksonen, M. Lawler, M. Leiminger, S. Mathot, O. Möhler, T. Nieminen, A. Onnela, T. Petäjä, F. M. Piel, P. Miettinen, M. P. Rissanen, L. Rondo, N. Sarnela, S. Schobesberger, K. Sengupta, M. Sipilä, J. N. Smith, G. Steiner, A. Tomè, A. Virtanen, A. C. Wagner, E. Weingartner, D. Wimmer, P. M. Winkler, P. Ye, K. S. Carslaw, J. Curtius, J. Dommen, J. Kirkby, M. Kulmala, I. Riipinen, D. R. Worsnop, N. M. Donahue and U. Baltensperger, *Nature*, 2016, **533**, 527–531.

8 E. M. Dunne, H. Gordon, A. Kürten, J. Almeida, J. Duplissy, C. Williamson, I. K. Ortega, K. J. Pringle, A. Adamov, U. Baltensperger, P. Barmet, F. Benduhn, F. Bianchi, M. Breitenlechner, A. Clarke, J. Curtius, J. Dommen, N. M. Donahue, S. Ehrhart, R. C. Flagan, A. Franchin, R. Guida, J. Hakala, A. Hansel, M. Heinritzi, T. Jokinen, J. Kangasluoma, J. Kirkby, M. Kulmala, A. Kupc, M. J. Lawler, K. Lehtipalo, V. Makhmutov, G. Mann, S. Mathot, J. Merikanto, P. Miettinen, A. Nenes, A. Onnela, A. Rap, C. L. S. Reddington, F. Riccobono, N. A. D. Richards, M. P. Rissanen, L. Rondo, N. Sarnela, S. Schobesberger, K. Sengupta, M. Simon, M. Sipilä, J. N. Smith, Y. Stozkhov, A. Tomé, J. Tröstl, P. E. Wagner, D. Wimmer, P. M. Winkler, D. R. Worsnop and K. S. Carslaw, *Science*, 2016, **354**, 1119–1124.

9 N. G. Adams, D. K. Bohme, D. B. Dunkin, F. C. Fehsenfeld and E. E. Ferguson, *J. Chem. Phys.*, 1970, **52**, 3133–3140.

10 M. E. Jacox and D. E. Milligan, *J. Mol. Spectrosc.*, 1974, **52**, 363–379.

11 J. T. Moseley, *J. Chem. Phys.*, 1976, **65**, 2512–2517.

12 R. A. Beyer and J. A. Vanderhoff, *J. Chem. Phys.*, 1976, **65**, 2313–2321.

13 D. E. Hunton, M. Hofmann, T. G. Lindeman and A. W. Castleman, *J. Chem. Phys.*, 1985, **82**, 134–150.

14 J. T. Snodgrass, C. M. Roehl, P. A. M. van Koppen, W. E. Palke and M. T. Bowers, *J. Chem. Phys.*, 1990, **92**, 5935–5943.

15 J. C. Bopp, E. G. Diken, J. M. Headrick, J. R. Roscioli, M. A. Johnson, A. J. Midey and A. A. Viggiano, *J. Chem. Phys.*, 2006, **124**, 174302.

16 A. A. Viggiano, *Phys. Chem. Chem. Phys.*, 2006, **8**, 2557–2571.

17 A. A. Viggiano, A. J. Midey and A. Ehlerding, *Int. J. Mass Spectrom.*, 2006, **255**, 65–70.

18 G. Beig, S. Walters and G. Brasseur, *J. Geophys. Res.*, 1993, **98**, 12775.

19 I. Dotan, J. A. Davidson, G. E. Streit, D. L. Albritton and F. C. Fehsenfeld, *J. Chem. Phys.*, 1977, **67**, 2874–2879.

20 N. Schoon, C. Amelynck, P. Bultinck and E. Arijs, *Int. J. Mass Spectrom.*, 2002, **221**, 209–218.

21 F. C. Fehsenfeld, C. J. Howard and A. L. Schmeltekopf, *J. Chem. Phys.*, 1975, **63**, 2835–2841.

22 O. Möhler and F. Arnold, *J. Atmos. Chem.*, 1991, **13**, 33–61.

23 N. S. Shuman, D. E. Hunton and A. A. Viggiano, *Chem. Rev.*, 2015, **115**, 4542–4570.

24 I. Dotan, D. L. Albritton, F. C. Fehsenfeld, G. E. Streit and E. E. Ferguson, *J. Chem. Phys.*, 1978, **68**, 5414–5416.

25 M. L. Huertas and J. Fontan, *Atmos. Environ.*, 1982, **16**, 2521–2527.

26 H. Kawamoto and T. Ogawa, *Planet. Space Sci.*, 1984, **32**, 1223–1233.

27 K. Nagato, Y. Matsui, T. Miyata and T. Yamauchi, *Int. J. Mass Spectrom.*, 2006, **248**, 142–147.

28 J. Viidanoja, T. Reiner and F. Arnold, *Int. J. Mass Spectrom.*, 1998, **181**, 31–41.

29 J. Viidanoja, T. Reiner, A. Kiendler, F. Grimm and F. Arnold, *Int. J. Mass Spectrom.*, 2000, **194**, 53–68.

30 C. van der Linde, W. K. Tang, C.-K. Siu and M. K. Beyer, *Chem. – Eur. J.*, 2016, **22**, 12684–12687.

31 W. K. Tang, C. van der Linde, C.-K. Siu and M. K. Beyer, *J. Phys. Chem. A*, 2017, **121**, 192–197.

32 C. Guimbaud, D. Labonnette, V. Catoire and R. Thomas, *Int. J. Mass Spectrom.*, 1998, **178**, 161–171.

33 J. Lengyel, J. Med, P. Slavíček and M. K. Beyer, *J. Chem. Phys.*, 2017, **147**, 101101.

34 J. Lengyel, M. Ončák, J. Fedor, J. Kočišek, A. Pysanenko, M. K. Beyer and M. Fárník, *Phys. Chem. Chem. Phys.*, 2017, **19**, 11753–11758.

35 J. Lengyel, C. van der Linde, A. Akhgarnusch and M. K. Beyer, *Int. J. Mass Spectrom.*, 2017, **418**, 101–106.

36 M. J. Frisch, G. W. Trucks, H. B. Schlegel, G. E. Scuseria, M. A. Robb, J. R. Cheeseman, G. Scalmani, V. Barone, G. A. Petersson, H. Nakatsuji, X. Li, M. Caricato, A. Marenich, J. Bloino, B. G. Janesko, R. Gomperts, B. Mennucci, H. P. Hratchian, J. V. Ortiz, A. F. Izmaylov, J. L. Sonnenberg, D. Williams-Young, F. Ding, F. Lipparini, F. Egidi, J. Goings, B. Peng, A. Petrone, T. Henderson, D. Ranasinghe, V. G. Zakrzewski, J. Gao, N. Rega, G. Zheng, W. Liang, M. Hada, M. Ehara, K. Toyota, R. Fukuda, J. Hasegawa, M. Ishida, T. Nakajima, Y. Honda, O. Kitao, H. Nakai, T. Vreven, K. Throssell, J. A. Montgomery, Jr., J. E. Peralta, F. Ogliaro, M. Bearpark, J. J. Heyd, E. Brothers, K. N. Kudin, V. N. Staroverov, T. Keith, R. Kobayashi, J. Normand, K. Raghavachari, A. Rendell, J. C. Burant, S. S. Iyengar, J. Tomasi, M. Cossi, J. M. Millam, M. Klene, C. Adamo, R. Cammi, J. W. Ochterski, R. L. Martin, K. Morokuma, O. Farkas, J. B. Foresman and D. J. Fox, *Gaussian 09, Revision A.02*, 2016.

37 R. F. Höckendorf, O. P. Balaj, C. van der Linde and M. K. Beyer, *Phys. Chem. Chem. Phys.*, 2010, **12**, 3772–3779.

38 P. Kofel, M. Allemann, H. Kellerhals and K. P. Wanczek, *Int. J. Mass Spectrom. Ion Processes*, 1986, **72**, 53–61.
39 C. Berg, T. Schindler, G. Niedner-Schatteburg and V. E. Bondybey, *J. Chem. Phys.*, 1995, **102**, 4870–4884.
40 S. Maruyama, L. R. Anderson and R. E. Smalley, *Rev. Sci. Instrum.*, 1990, **61**, 3686–3693.
41 V. E. Bondybey and J. H. English, *J. Chem. Phys.*, 1981, **74**, 6978–6979.
42 T. G. Dietz, M. A. Duncan, D. E. Powers and R. E. Smalley, *J. Chem. Phys.*, 1981, **74**, 6511–6512.
43 D. de Jesus Medeiros and A. S. Pimentel, *J. Phys. Chem. A*, 2011, **115**, 6357–6365.
44 A. Akhgarnusch, R. F. Höckendorf and M. K. Beyer, *J. Phys. Chem. A*, 2015, **119**, 9978–9985.
45 O. P. Balaj, C. B. Berg, S. J. Reitmeier, V. E. Bondybey and M. K. Beyer, *Int. J. Mass Spectrom.*, 2009, **279**, 5–9.
46 T. E. Cooper, J. T. O'Brien, E. R. Williams and P. B. Armentrout, *J. Phys. Chem. A*, 2010, **114**, 12646–12655.
47 R. C. Dunbar, *J. Phys. Chem.*, 1994, **98**, 8705–8712.
48 R. C. Dunbar, *Mass Spectrom. Rev.*, 2004, **23**, 127–158.
49 R. C. Dunbar and T. B. McMahon, *Science*, 1998, **279**, 194–197.
50 B. S. Fox, M. K. Beyer and V. E. Bondybey, *J. Phys. Chem. A*, 2001, **105**, 6386–6392.
51 A. Kamariotis, O. V. Boyarkin, S. R. Mercier, R. D. Beck, M. F. Bush, E. R. Williams and T. R. Rizzo, *J. Am. Chem. Soc.*, 2006, **128**, 905–916.
52 E. N. Kitova, D. R. Bundle and J. S. Klassen, *J. Am. Chem. Soc.*, 2002, **124**, 5902–5913.
53 S. W. Lee, P. Freivogel, T. Schindler and J. L. Beauchamp, *J. Am. Chem. Soc.*, 1998, **120**, 11758–11765.
54 T. Schindler, C. Berg, G. Niedner-Schatteburg and V. E. Bondybey, *Chem. Phys. Lett.*, 1996, **250**, 301–308.
55 P. D. Schnier, W. D. Price, R. A. Jockusch and E. R. Williams, *J. Am. Chem. Soc.*, 1996, **118**, 7178–7189.
56 M. Sena and J. M. Riveros, *Rapid Commun. Mass Spectrom.*, 1994, **8**, 1031–1034.
57 D. Thölmann, D. S. Tonner and T. B. McMahon, *J. Phys. Chem.*, 1994, **98**, 2002–2004.
58 R. L. Wong, K. Paech and E. R. Williams, *Int. J. Mass Spectrom.*, 2004, **232**, 59–66.